16th World Conference on Earthquake Engineering, 16WCEE 2017
Santiago Chile, January 9th to 13th 2017
Paper N° 4943
Registration Code: S-H1464447916

TOWARDS A GEOPHYSICAL CHARACTERIZARION OF THE CHILEAN STRONG-MOTION STATIONS

F. Leyton[1], C. Pastén[2], G. Montalva[3], G. Hurtado[4] , A. Leopold[5], S. Ruiz[6] , E. Saéz[7]

[1] Senior Seismologist, Universidad de Chile, leyton@csn.uchile.cl
[2] Assistant Professor, Universidad de Chile, cpasten@ing.uchile.cl
[3] Assistant Professor, Universidad de Concepción, gmontlva@udec.cl
[4] Field Engineer, Universidad de Chile, ghurtado@csn.uchile.cl
[5] Field Engineer, Universidad de Chile, aleopold @csn.uchile.cl
[6] Assistant Professor, Universidad de Chile, sruiz@dgf.uchile.cl
[7] Associate Professor, P. Universidad Católica de Chile, esaez@ing.puc.cl

Abstract

The Chilean Seismological Networks has been rapidly growing these past years, going from few dozens of stations, to nearly a 100 installed all over the country. Even more, this network is complemented by the Accelerographic National Network, with nearly 300 strong-motion stations, deployed on a large effort by the National Office of Emergencies (Onemi), in a variety of cities and site conditions all over the country. All of these stations are currently providing very useful information of the earthquakes that take place in Chile, and are expected to record moderate to large events. However, the lack of appropriate site characterization sets an important limit to its usefulness. In the present work, we propose a methodology to begin a geophysical characterization of all of these stations, based on array measurements of microtremors and horizontal-to-vertical spectral ratios. In the present work, we present some preliminary results for some stations located in Valparaíso, Coquimbo, Tarapacá, and the Metropolitan regions. This information will help improve our understanding of the behavior of soils during an earthquake, providing relevant information for seismic codes.

Keywords: geophysical characterization, strong-motion stations, microtremors, surface wave methods

1. Introduction

Chilean Seismic Network has been growing not only in number of stations, but also in the instruments that they have. Currently, the National Seismological Center (CSN) is operating more than 100 stations, composed of broadband seismometers, accelerometers, and GNSS instruments, with their data being transmitted in real-time to the analysis center [1]. Even more, recently the National Office of Emergency and Mitigations (Onemi, for its Spanish initials) has transferred nearly 300 strong-motion stations to the CSN, to be operated along with the rest of the network. These instruments (RNA network) are located through out the whole country, mostly concentrated on cities and other populated localities; this gives a unique opportunity to increase the knowledge of the behavior of the soils during earthquakes, especially in those places where there is concentration of population. Note that all the data collected by these networks is freely available and can be downloaded at any time [2]. Moreover, the CSN is currently beginning a large effort to characterize the local site conditions where these stations are located.

It has been clearly established that local site conditions strongly modify the movements produced by large earthquakes; even more, it has been clearly observed that damage produced by large earthquakes is strongly controlled by these conditions [3]. Currently, several seismic codes have adopted a number of geophysical measurements for classification related to seismic site amplifications, being the average of the upper 30 meters of the S wave profile (Vs_{30}) the most popular. Furthermore, recent studies suggests that these characteristics, being useful in most cases, fail to capture the effect of thick sediments covers [4] and might even overestimate the ground motion amplitudes for a given frequency range [5], having the need to complement them with other sources of information, such as the predominant site frequency [6].

Several methods have been used to determine the properties of the upper layers in a site, ranging from invasive and non-invasive methods. These last ones have particularly preferred due to their lower costs and

interesting capabilities of describing the subsurface structure [7,8,9]. In the present study, we focus on array-based, surface wave methods, shown to be able to perform correctly in Chile [10,11,12]. We complement these procedures with the well-known horizontal-to-vertical spectral ratio, becoming increasingly popular and quite inexpensive [12,13,14,15], and have been successfully used to estimate the fundamental frequency of the site. In the present study, we use microtremors measurements to estimate the geophysical properties of the upper layers of the sites with strong-motion stations. We focus on the methodologies that enable us to investigate up to a significant depth and can be used in urban areas, with strong influence of anthropogenic seismic noise.

2. Data

In the present study, we investigated the dynamic properties of the sites where strong-motion stations are located, mostly in midsize to large cities. So far, we have only studied stations from the RNA, from its Spanish name: *Red Nacional de Acelerógrafos*. This network was deployed by the Chilean National Emergency Office, Onemi, and recently has been given to the National Seismic Center for its oversight. Here we have investigated some stations from the Metropolitan, the Coquimbo, and the Valparaíso regions, as shown in Fig. 1; details on its location can be found in Table 1. Some of these stations have been deployed since 2013, having successfully recorded events ever since. In addition, some of these stations were able to record the motions from the 2015 Mw 8.3 Illapel earthquake [2].

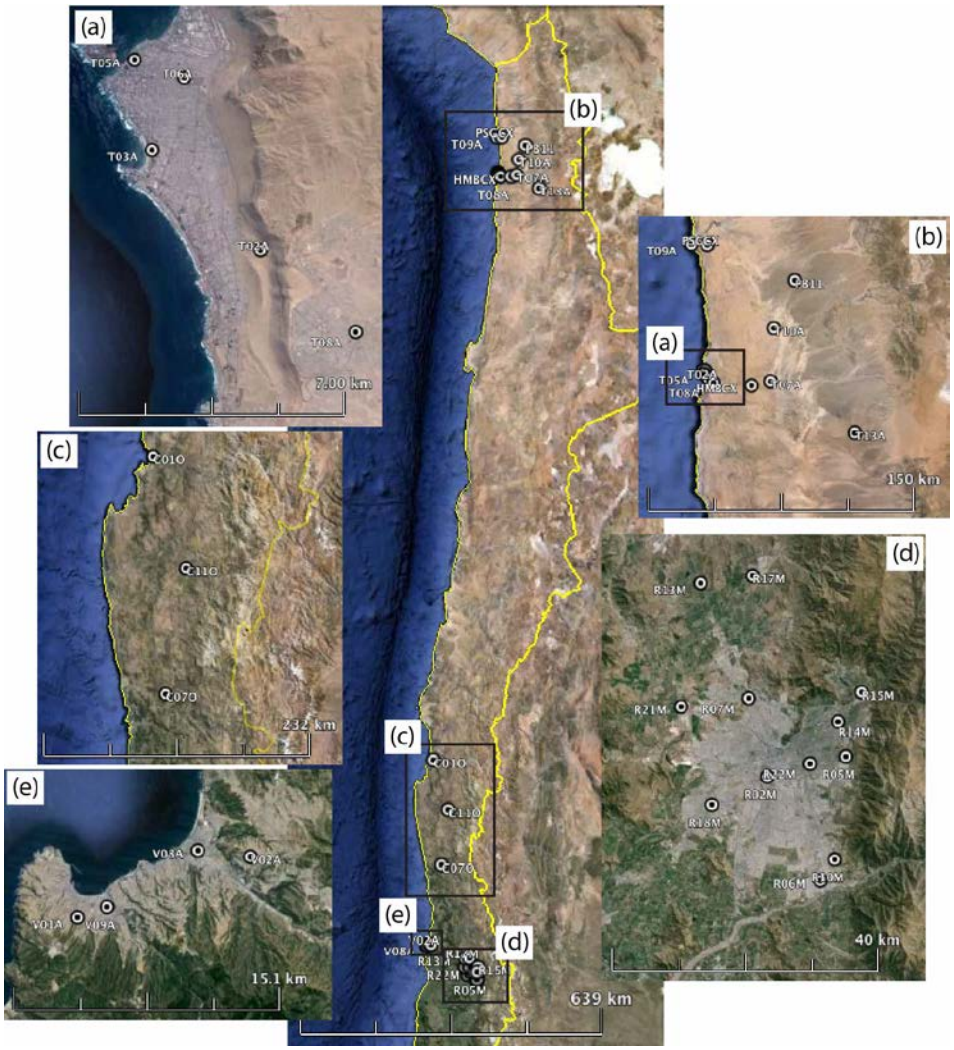

Fig. 1 – Google Earth images showing the stations investigated in this study: (a) Iquique, (b) Tarapacá, (c) Coquimbo, (d) Metropolitan, and (e) Valparaíso; each dot represents a station and the names correspond to its code name.

The locations of the stations are presented in Table 1; in this same Table we also show the obtained values of the average velocity in the upper 30 meters (Vs_{30}) and the classification from the horizontal-to-vertical spectral ratio (HVSR class), both of them explained in the following sections.

Table 1 – Location of the stations considered in this study and some results, see text for details.

Station Code	Longitud [°]	Latitud [°]	Vs_{30} [m/s]	HVSR class
C01O	-71.2379	-29.8770	510.8	s_V A
C07O	-71.1675	-31.6336	654.7	s_{II} B
C11O	-70.9589	-30.6964	626.4	s_{III} A
V01A	-33.0531	-71.6220	606.6	s_{II} B
V02A	-33.0231	-71.5178	595.3	s_{II} C
V08A	-33.0198	-71.5498	343.8	s_V C
V09A	-33.0482	-71.6045	212.6	s_V B
T02A	-20.2524	-70.1181	269.3	s_{IV} C
T03A	-20.2303	-70.1459	613.1	s_{II} B
T05A	-20.2097	-70.1502	1024.9	s_I
T06A	-20.2142	-70.1378	1257.6	s_I
T07A	-20.2562	-69.7860	326.2	s_{III} B
T08A	-20.2700	-70.0941	985.9	s_I
T09A	-19.5957	-70.2108	1585.8	s_I
T10A	-19.9954	-69.7671	335.6	s_{III} A
T13A	-20.4963	-69.3375	377.9	s_{III} A
HMBCX	-20.2782	-69.8879	742.7	s_I
PSGCX	-19.5972	-70.1231	1641.3	s_I
PB11	-19.7610	-69.6557	1048.5	s_V A
R02M	-70.6599	-33.4707	724.3	s_I
R05M	-70.5340	-33.4429	634.7	s_I
R06M	-70.5745	-33.6070	594.4	s_{III} A
R07M	-70.6898	-33.3673	270.9	s_V B
R10M	-70.5515	-33.5788	450.3	s_{III} A
R13M	-70.7669	-33.2155	280.5	s_{IV} B
R14M	-70.5463	-33.3971	574.0	s_I
R15M	-70.5084	-33.3578	374.3	s_I
R17M	-70.6838	-33.2055	562.0	s_{II} A
R18M	-70.7488	-33.5084	370.3	s_{III} B
R21M	-70.7983	-33.3789	355.1	s_V C
R22M	-70.5916	-33.4530	647.8	s_I

3. Methodology

For this study, we have used mostly passive Surface Wave Methods [7,8,9,10,11,12], focusing our efforts on arrays measurements, and complement them with single-station measurements, such as horizontal-to-vertical spectral ration (HVSR). For array methods, we have extensively used SPAC [7] and its recent extensions [16,17,18]; an example will be discussed below. For all the measurements, we used 3-components, 4.5-Hz, geophones [19]; these instruments have shown their suitability for these kinds of studies [10,12,15]. In the present study, we only used the vertical components for the array processing, while the horizontal ones were only used to compute the horizontal-to-vertical spectral ratios. This was made following a previously defined procedure [20] making use of the Stockwell Transform (ST) [21]. In few words, we divide the complete time window (usually 20 to 40 minutes long) in 60 sec subwindows, each one processed in the same ways. We obtain the ST of each trace and compute the total horizontal energy by adding the amplitude horizontal components, without phase. Next, for each time step, we compute the horizontal-to-vertical spectral ratio (HVSR), for a frequency range from 0.1 to 10 Hz. Finally, we find the percentiles that exceed certain value, obtaining a robust estimation of the median of the HVSR. Some examples can be seen in Fig. 2.

Following the recent work of Idini and colleagues [22], we classify all our HVSR results considering the observed predominant period and amplitude; this kind of classification has been previously applied to strong-motion stations in Iran [23,24], Taiwan [25], Japan [26,27], and Italy [28]. It basically considers the observed predominant frequency and the HVSR amplitude as shown in Table 2, right and left. Considering the predominant frequency, a softer site class is given for sites with lower frequencies, ranging from s_{II} up to s_V; in case of more than one peak, the largest one is selected. In the present study, we have limited the observed values to the frequency range previously fixed between 0.1 an 10 Hz, and have computed the HVSR from the ST of microtremors recording while Idini et al. [22] consider the 5%-damping, response spectra of acceleration records. Note that site classification s_I corresponds to a stiff soil with HVSR amplitude lower than 2 and cannot be related to any predominant frequency.

Table 2 – Site classification considering HVSR results: left table considers the observed predominant frequency and the right table, its corresponding amplitude (modified from [22]).

Site Class	Frequency Limits [Hz]	
	Lower	Upper
s_{II}	5.00	10.00
s_{III}	2.50	5.00
s_{IV}	1.25	2.50
s_V	0.10	1.25

Site Class	HVSR amplitude limits	
	Lower	Upper
s_I	-	2
A	2	3
B	3	4
C	4	-

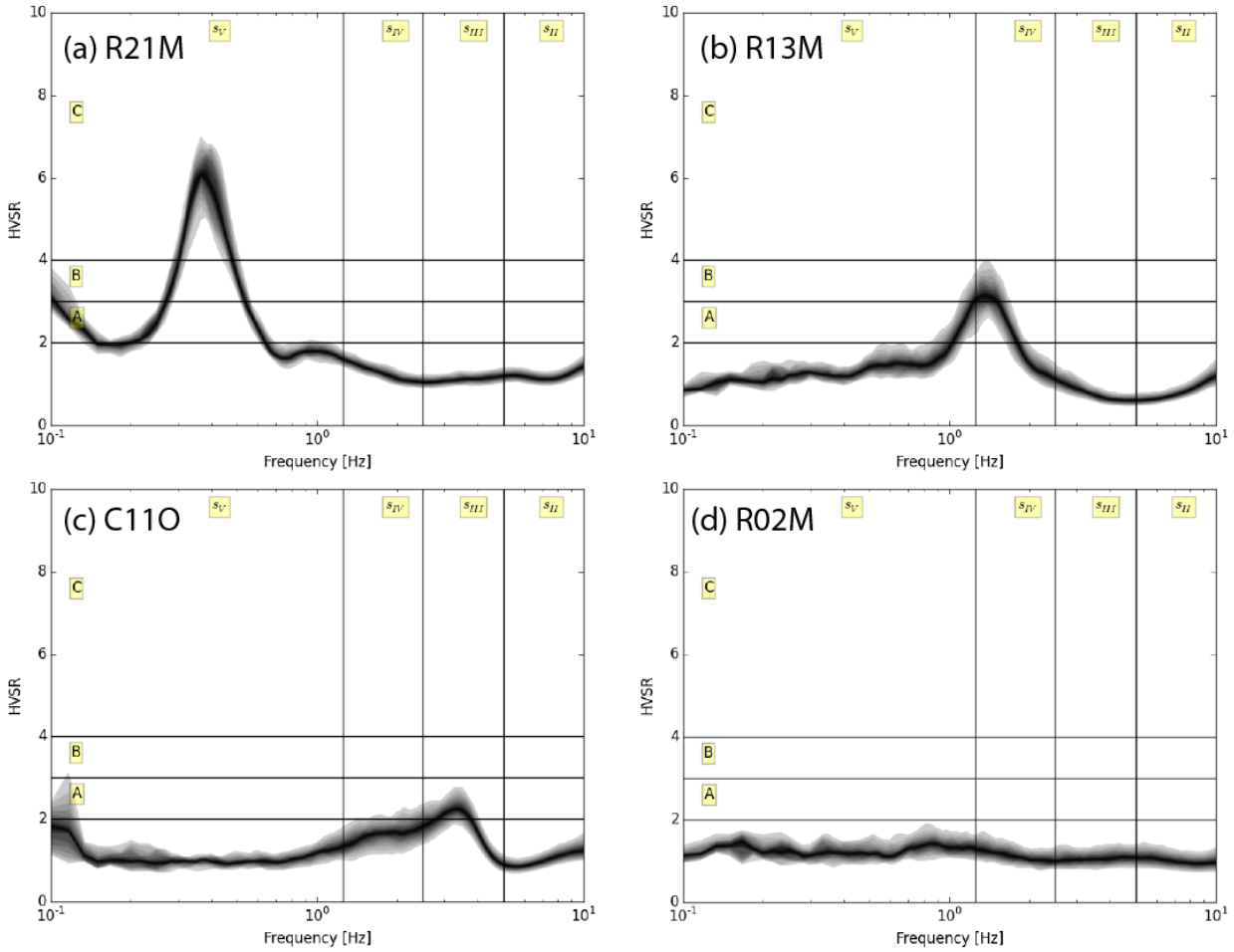

Fig. 2 – Examples of horizontal-to-vertical spectral ratio (HVSR) considering the S Transform for: (a) R21M, (b) R13M, (c) C11O, and (d) R02M. The graphs also show the classification defined in [22], see text for details.

For the array measurements, we first deploy the geophones near the strong-motion station, trying to define the largest aperture array in its vicinity, as shown in Fig. 3. Next, according to space availability, we performed a larger array in the nearby area, as shown in the same Fig. We did microtremors measurements for 20 to 40 minutes, depending on the noise level at the time of the measurements. For sites where rock was suspected to be near the surface, given the location on top of a hill, we complemented the passive measurements using active source methods, methodology that has proven to give enough information to estimate the upper 30 to 50 meters [10].

Fig. 3 – Google Earth maps showing examples of the geometry used in the array measurements, these come from the C01O station: each yellow square shows the location of a geophone and the white circle represents the strong-motion station.

In the present study, we mainly used the methodology first proposed by Aki [7], and later modified for more general configurations [29,30]. This methodology has shown to be able to explore the characteristics of the dispersion curves in the lower frequency range considered [10]. Furthermore, we complement these results with the method recently proposed by Erkström and colleagues [16,17], who noticed that the same methodology can be further used to higher frequencies, by focusing on the zero-crossings [18]. Following Erkström et al [16,17], the phase velocity at a frequency ω_n, where we have a zero-crossing, $c(\omega_n)$ can be computed using:

$$c(\omega_n) = \omega_n \, r/z_{n+m} \qquad (1)$$

where r is the distance between the sensors and z_{n+m} is the n+m zero-crossing of the Bessel function of order 0; these values can be easily obtained from tables. An example is shown in Fig. 4: the upper panel shows the Bessel Function of order 0, the red circles mark the zero-crossing; while the lower panel shows the corresponding phase velocities by considering different possible values of m, shown at the upper-right corner. For this particular case, the appropriate values corresponds to m=0, giving the correct dispersion curve.

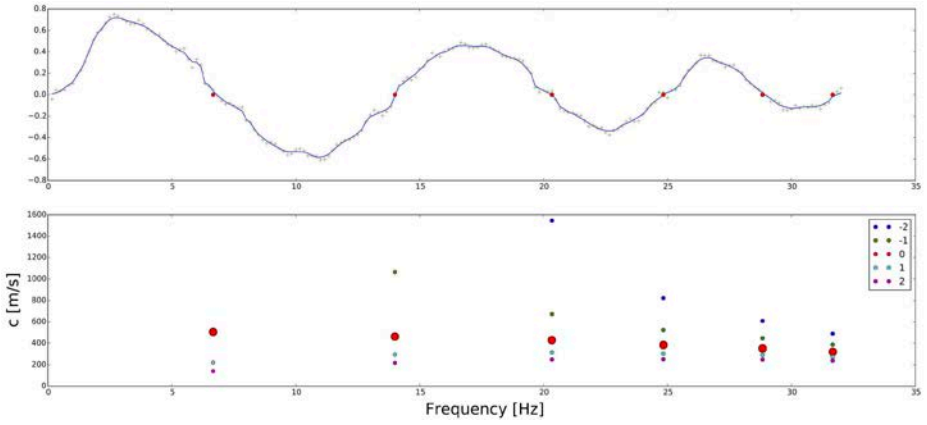

Fig. 4 – Results for R21M. Top panel: result of the correlation function, each green cross is an observed results while the blue curve shows a smoothed version of it; the red dots mark the zero-crossing. Lower panel: given the zero-crossing, and considering different values of m (see equation (1)), shown in the upper right corner, the phase velocity is computed.

As mentioned before, the lower frequency range of the dispersion curve is obtained using SPAC, mostly considering its generalization to different geometries made by Chavez-García and colleagues [29,30]; in the present study, we used the implementation made by Wathelet and colleagues [31] in the open source, freely available software, Geopsy. An example is presented in Fig. 5, left panel. This panel presents the corresponding dispersion curve for the lower end of the frequency range. In addition, the results from the zero-crossings estimation are shown for higher frequencies (above 4 Hz). To the right, the 2 graphs show the used Bessel Functions of order 0, with its corresponding error bar.

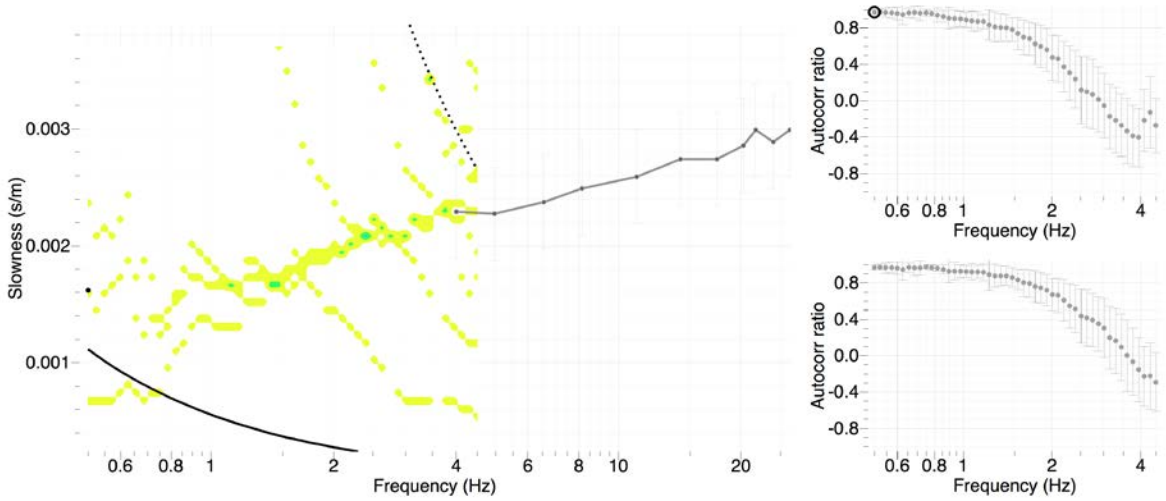

Fig. 5 – Results for R21M. Left: example of dispersion curve formed by combining SPAC results, for lower frequencies, and the zero-crossing technique, for higher frequencies. Right: examples of correlation function for 2 rings, related to the dispersion curve shown on the left.

Finally, the inversion from the obtained dispersion curves to the S-wave velocity profile was performed using the Neighborhood Algorithm [32], appropriately adapted for this case by Wathelet [33,34]. We verified each inversion by comparing the observed HVSR with the predicted ellipticity ratio, obtained for the best Vs model in each case.

4. Results

In the present study we performed microtremors measurements in several strong-motion stations located in Coquimbo, Valparaíso, Tarapacá, and Metropolitan regions. We were able to successfully determine the S-wave velocity (Vs) in the upper layers, extend up to 50 meters, in average. The obtained profiles are presented in Fig. 6 to 9. In all of these Figs., the color is proportional to the obtained misfit of the dispersion curve, following the corresponding scale in the lower part of each graph; in black are shown the models with the lower misfit. All of the profiles are plotted to a depth of 50 m; however, the horizontal scale showing the Vs values vary in each profile depending on the observed values. Each graph is labeled with the station code, as shown in Fig. 1 and Table 1; the Vs_{30} calculated from the profiles are also shown in the same Table.

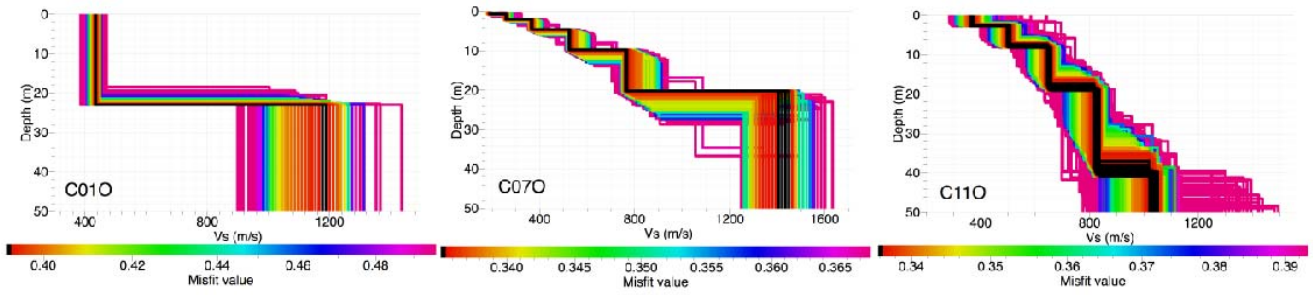

Fig. 6 – S-wave velocity profiles for the stations in Coquimbo region; each one is labeled with the corresponding code name. For each graph, the color is proportional to the misfit of the model, following the scale below each one; black shows the best models.

From Fig. 6 we can see that station C01O presents rather large Vs values (higher than 400 [m/s]) but it's classified as s_V A, a rather low value (see Table 1). This low predominant frequency is produced by the strong impedance contrast at 23 m depth, having an increase in Vs from 430 [m/s] to almost 1200 [m/s]. On the other hand, station C07O shows increasing values of Vs from 200 to 760 [m/s], with a final jump to more than 1400 [m/s]; these large Vs values create the high frequency peak that defines the classification to s_{II} B. In the same way, station C110 presents a clear increment in Vs values, but in a much lower rate, reaching more than 1000 [m/s] below 40 m depth; this lower rate is responsible of the lower predominant frequency observed, classifying as s_{III} A.

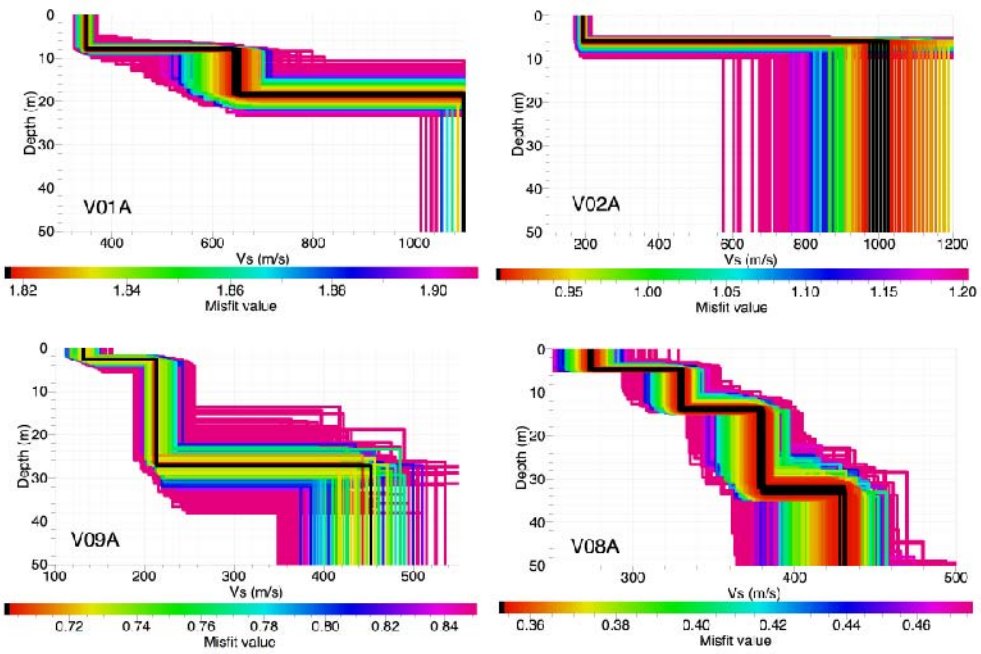

Fig. 7 – S-wave velocity profiles for the stations in Valparaíso region; see Fig. 6 and text for details.

Fig. 7 shows stations V01A and V02A with lower Vs values in the upper layer, but jumping to larger velocities (over 1000 [m/s]) in the few upper meters; this can be explained by their location in a strongly weathered rock, in the Valparaíso and Viña de Mar hills. These thin upper layers produce the large predominant frequencies observed, classifying both as s_{II}. On the other hand, V09A and V08A are located down in the Valparaíso and Viña del Mar valleys, respectively, placed on much softer materials, with Vs values usually below 400 [m/s]. These softer materials produce the lower predominant frequencies, relating them to s_V classification.

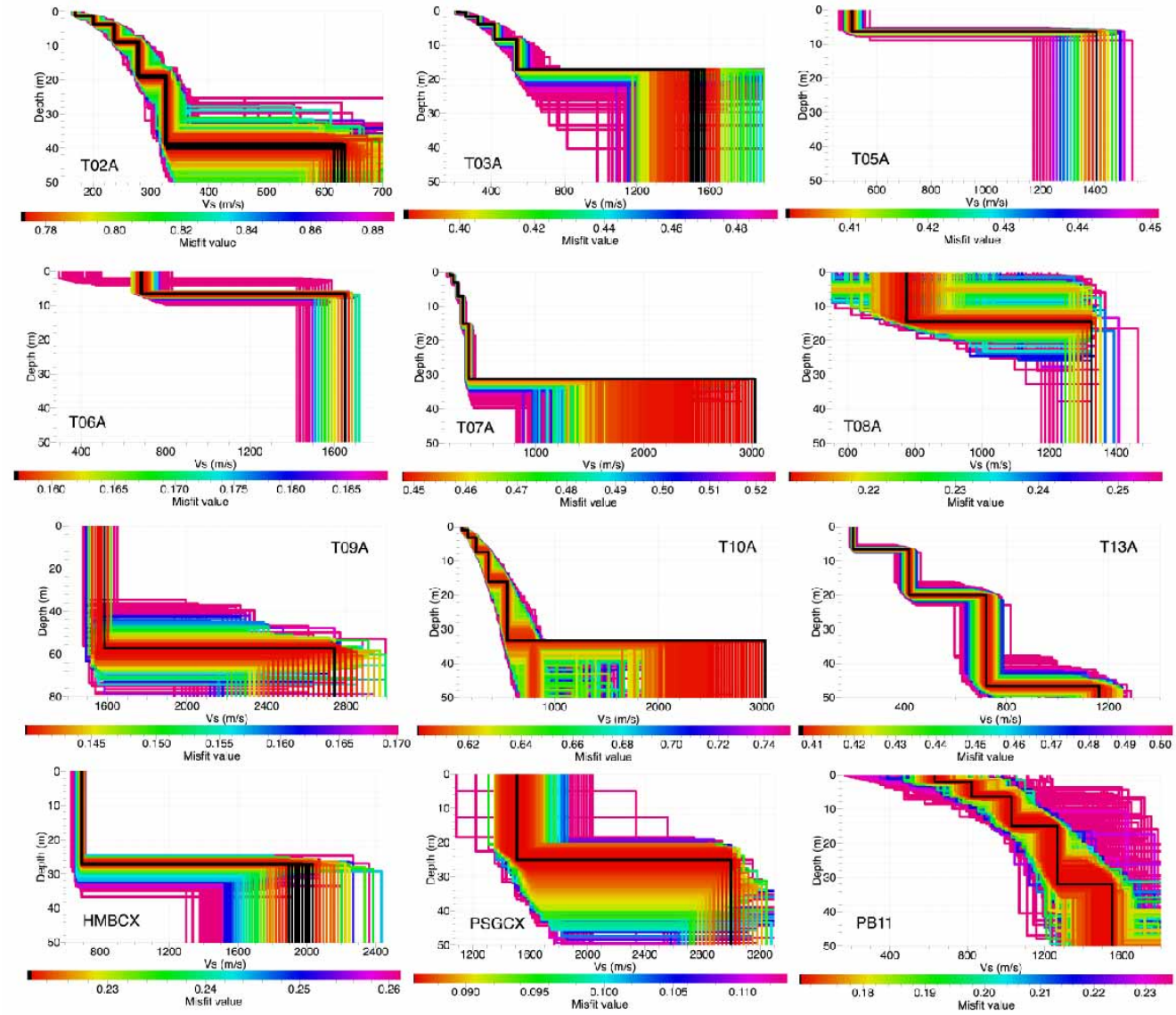

Fig. 8 – S-wave velocity profiles for the stations in Tarapacá region; see Fig. 6 and text for details.

Fig. 8 shows that stations T02A, T07A, T10A, and T13A are characterized by low velocities in the upper layers (less than 400 [m/s]) and a strong impedance contrast below, producing a clear peak at low frequencies; hence, classifying as s_{IV} and s_{III} from HVSR. On the other hand, stations T05A, T06A, T08, T09A, and HMBCX, like stations V01A and V02A in the previous case, show a thin layer with rather low velocities followed by layers of high Vs values, producing large predominant frequencies that go above the limit used in this study (10 [Hz]), leaving them as a s_I classification. Station PSGCX shows a similar behavior, having a strong velocity change in the upper meters, but it starts at a much larger velocity in the upper layer.

Station T03A is characterized by low velocities in the upper layers and a strong impedance contrast in the upper meters, leading to a high predominant frequency, reflected in its classification as s_{II}. Finally, station PB11 shows a slow increase in velocity from large Vs values (600 [m/s]) to even larger (over 1500 [m/s]); however, it's classified as s_V A, quite a low predominant frequency. We believe that this is produced by a small impedance contrast that was not observed with the measurements made, being a much lower depths; nevertheless, this is issue should be further explored.

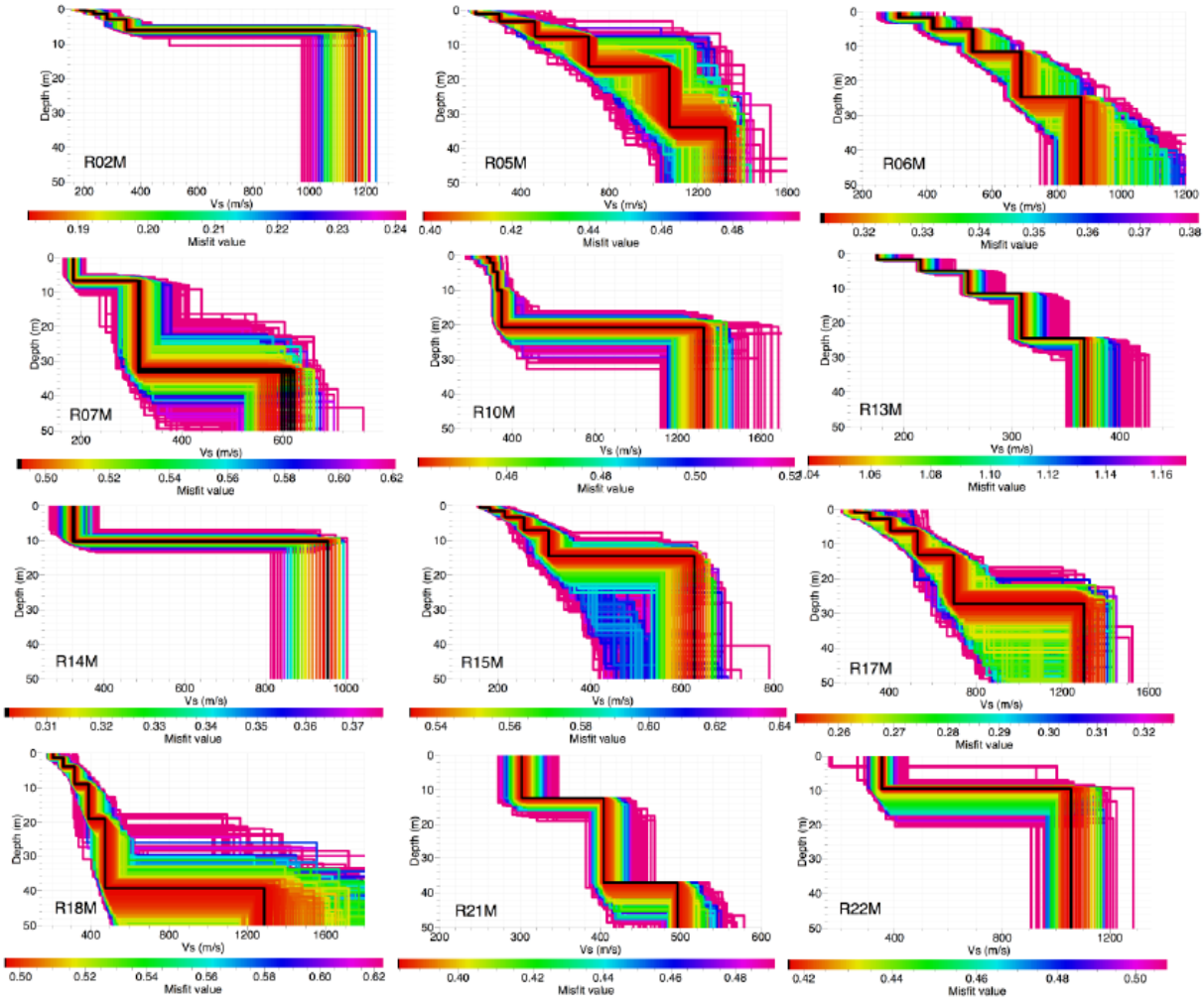

Fig. 9 – S-wave velocity profiles for the stations in Metropolitan region; see Fig. 6 and text for details.

From Fig. 9, note that stations R02M, R14M, and R22M classify as s_I from the HVSR, meaning that no predominant frequency is observed; however, these stations present a clear velocity contrast in the in the upper 10 m. This is explained by the fact that in this study we restrict the frequency range up to 10 [Hz], and the profiles for these three stations produce a clear predominant frequency at larger values, not shown in our classification scheme, just as observed in station V01A, V02A, T05A, T06A, T08, T09A, and HMBCX, of previous cases. Another intersting case is presented by R05M: the HVSR classification defines it as a s_I soil, but in the upper layer we found S wave velocities as low as 200 m/s. This is produced by the slow increase in velocity with depth, not presenting any strong impedance contrast that could produce a peak in the frequency range considered in this study (from 0.1 to 10 [Hz]). The rest of the cases can be explained in similar ways as done before.

5. Conclusions

In this study, we present a methodology to retrieve the geophysical properties of site where strong-motion stations are located. This issue is particularly difficult due to the fact that most of these stations are located in moderate-to-large cities, with high urban noise. We successfully explore stations in the Coquimbo, the Valparaíso and the Metropolitan regions, being able to explore up to 50 meters depth. We accomplish this using array-based and 3-component, microtremors measurements using 4.5-Hz geophones. The most reliable methods

used in the present study were SPAC [7] and it's extension to higher frequency considering only the zero-crossings [16,17]. We believe that this information will contribute in the understanding of the strong motion shaking produce from large to moderate earthquakes, especially in sites where most of the Chilean population lives.

6. Acknowledgements

The authors would like to thank the Geopsy Team for making freely available its software for the processing of microtremors [31]. We also would like to thank C. Benitez, S. Droguett, L. Podestá, and P. Troncoso for their help during the Tarapacá campaign and J. Salomón for his help during the Coquimbo campaign.

7. Copyrights

8. References

[1] National Seismological Center, Universidad de Chile: www.csn.uchile.cl.

[2] Strong motion database: evtdb.csn.uchile.cl, managed by the National Seismological Center.

[3] Seed HB, Ugas C, Lysmer J (1976): Site-dependent spectra for earthquake-resistant design, *Bull. Seism. Soc. Am.* **66,** 221–243.

[4] Steidl, J. H. (2000). Site response in Southern California for probabilistic seismic hazard analysis, Bull. Seismol. Soc. Am. 90, 149–169.

[5] Park D., Hashash YMA (2004): Probabilistic seismic hazard analysis with nonlinear site effects in the Mississippi embayment, *Proc. 13th World Conf. Earthq. Eng*. Vancouver, British Columbia, Canada, 1–6 August 2004, CD-Rom Edition, paper no. 1549.

[6] Cadet H, Bard PY, Rodriguez-Marek A (2010): Defining a standard rock site: Propositions based on the KiK-net database, *Bull. Seismol. Soc. Am.* 100, 172–195.

[7] Aki K (1957): Space and time spectra of stationary stochastic waves, with special reference to microtremors. *Bull. Earthq. Res. Inst.* 35, 415–457.

[8] Asten MW, Henstridge JD (1984) Array estimators and use of microseisms for reconnaissance of sedimentary basins, *Geophysics*, **49,** 1828–1837.

[9] Horike M (1985) Inversion of phase velocity of long-period microtremors to the S-wave-velocity structure down to the basement in urbanized areas, *J. Phys. Earth*, **33,** 59–96.

[10] Humire F, Sáez E, Leyton F, Yañez G (2014): Combining active and passive multi- channel analysis of surface waves to improve reliability of $V_{S,30}$ estimation using standard equipment, *Bull Earthquake Eng*, doi 10.1007/s10518-014-9662-5.

[11] Kayen R, Carkin BD, Corbet S, Pinilla C, Ng A, Gorbis E, Truong C (2014): Seismic velocity site characterization of thirty-one Chilean seismometer stations by spectral analysis of surface wave dispersion. *Technical Report PEER 2014/05*, Pacific Earthquake Engineering Research, Berkeley, USA.

[12] Molnar S, Ventura CE, Boroschek R, Archila M (2015): Site characterization at Chilean strong-motion stations: Comparison of downhole and microtremor shear-wave velocity methods. *Soil Dynamics and Earthquake Engineering*, 79 (2015) 22–35.

[13] Pilz M, Parolai S, Picozzi M, Wang R, Leyton F, Campos J, Zschau J (2010): Shear wave velocity model of the Santiago de Chile basin derived from ambient noise measurements: a comparison of proxies for seismic site conditions and amplification, *Geophys. J. Int*., 182, 355–367, doi: 10.1111/j.1365-246X.2010.04613.x

[14] Leyton, F., S. Ruiz, S.A. Sepúlveda, J.P. Contreras, S. Rebolledo, M. Astroza (2013) Microtremors' HVSR and its correlation with surface geology and damage observed after the 2010 Maule earthquake (Mw 8.8) at Talca and Curicó, Central Chile, *Engineering Geology*, doi: 10.1016/j.enggeo.2013.04.009.

[15] Becerra, A., L., Podestá, R. Monetta, E. Sáez, F. Leyton, G. Yañez (2015) Seismic microzoning of Arica and Iquique, Chile, *Natural Hazards*, doi 10.1007/s11069-015-1863-y.

[16] Ekström, G., Abers, G.A., Webb, S.C., 2009. Determination of surface-wave phase velocities across USArray from noise and Aki's spectral formulation. *Geophys. Res. Lett*. 36 (18), 5–9.

[17] Ekström, G., 2014. Love and rayleigh phase-velocity maps, 5–40 s, of the western and cen- tral USA from USArray data. *Earth Planet. Sci. Lett*. 402, 42–49.

[18] Pastén C, Sáez M, Ruiz S, Leyton F, Salomón J, Poli P (2016): Deep characterization of the Santiago Basin using HVSR and cross-correlation of ambient seismic noise, *Engineering Geology*, 201, 57–66.

[19] Tromino ® from Moho, Science & Technology: www.tromino.eu

[20] Leyton F, Ruiz S, Astroza M (2012) Correlation between seismic intensity for the Maule 2010 earthquake (Mw 8.8) and microtremors' HVSR, *15th World Conference on Earthquake Engineering*, Lisboa Portugal.

[21] Stockwell RG, Mansinha L, Lowe RP (1996): Localization of the complex spectrum: the S transform. *IEEE Trans. Signal Process.*, 44, 998–1001.

[22] Idini B, Rojas F, Ruiz S, Pastén C (2016) Ground motion prediction equations for the Chilean subduction zone, in preparation.

[23] Zaré M, Bard P-Y, Ghafory-Ashtiany M. (1999): Site characterizations for the Iranian strong motion network. *Soil Dyn Earthq Eng*;18:101–23.

[24] Ghasemi H, Zare M, Fukushima Y, Sinaeian F. (2009) Applying empirical methods in site classification, using response spectral (H/V): a case study on Iranian strong motion network (ISMN). *Soil Dyn Earthq Eng*, 29:121–32.

[25] Lee C-T, Cheng C-T, Liao C-W, Tsai Y-B. (2001): Site classification of Taiwan free-field strong-motion stations. *Bull Seismol Soc Am*, 91:1283–97.

[26] Yamazaki F, Ansary MA. (1997): Horizontal-to-vertical spectrum ratio of earthquake ground motion for site characterization. *Earthq Eng Struct Dyn*, 1997;26:671– 89.

[27] Zhao JX, Zhang J, Asano A, Ohno Y, Oouchi T, Takahashi T, Ogawa H, Irikura K, Thio HK, Somerville PG, Fukushima Y, Fukushima Y. Attenuation relations of strong ground motion in Japan using site classification based on predominant period. Bull Seismol Soc Am 2006;96:898–913.

[28] Di Alessandro C, Bonilla LF, Boore DM, Rovelli A, Scotti O. (2012): Predominant-period site classification for response spectra prediction equations in Italy. *Bull Seismol Soc Am*;102:680–95.

[29] Chávez-García F, Rodríguez M, Stephenson W (2005): An alternative approach to the SPAC analysis of microtremors: exploiting stationarity of noise. *Bull Seismol Soc Am* ,95:277–293.

[30] Chávez-García F, Rodríguez M, Stephenson W (2006): Subsoil structure using SPAC measurements along a line. *Bull Seismol Soc Am*, 96:729–736

[31] Wathelet M (2002–2011) GEOPSY packages (Version 2.5.0) [software]: retrieved from http://www.geopsy.org/download.php

[32] Sambridge, M., 1999. Geophysical inversion with a neighborhood algorithm: I. Searching a parameter space. Geophys. J. Int. 138, 479–494.

[33] Wathelet, M., 2005. Array Recordings of Ambient Vibrations: Surface-Wave Inversion. Liege University, Belgium.

[34] Wathelet, M., 2008. An improved neighborhood algorithm: parameter conditions and dynamic scaling. Geophys. Res. Lett. 35 (9).